Chou and Cheng *Earth, Planets and Space* (2017) 69:122
DOI 10.1186/s40623-017-0709-0

Earth, Planets and Space

FULL PAPER Open Access

Distribution of water-group ion cyclotron waves in Saturn's magnetosphere

Marty Chou[1*] and Chio Zong Cheng[2]

Abstract

The water-group ion cyclotron waves (ICWs) in Saturn's magnetosphere were studied using the magnetic field data provided by the MAG magnetometer on board the Cassini satellite. The period from January 2005 to December 2009, when the Cassini radial distance is smaller than 8 R_S, was used. ICWs were identified by their left-hand circularly polarized magnetic perturbations and wave frequencies near the water-group ion gyrofrequencies. We obtained the spatial distribution of ICW amplitude and found that the source region of ICWs is mostly located in the low-latitude region, near the equator and inside the 6 R_S radial distance. However, it can extend beyond 7 R_S in the midnight region. In general, the wave amplitude is peaked slightly away from the equator, for all local time sectors in both the Northern and Southern Hemispheres. By assuming that the water-group ions are composed of pickup ions and background thermal ions, we obtained the local instability condition of the ICWs and estimated their growth rate along the field lines. If the wave amplitude is correlated with the growth rate, the observed latitudinal dependence of the wave amplitude can be well explained by the local stability analysis. Also, latitudinal location of the peak amplitude is found to depend on the local time. This implies a local time dependence for the water-group ion parallel temperature $T_{\|}$, as determined from the theoretical calculations.

Keywords: Plasma waves and instabilities, Kinetic theory, Saturn, Ion cyclotron waves

Introduction

Ion cyclotron waves (ICWs) in Saturn's magnetosphere were identified in early reports of magnetometer data analysis from the Pioneer 11 and Voyager 1 missions (e.g., Smith and Tsurutani 1983; Barbosa 1993). Later studies using Cassini data showed that ICWs in the inner magnetosphere of Saturn are closely related to water-group ions (Dougherty et al. 2004, 2005; Leisner et al. 2005, 2011). They are suggested to be generated by newly picked up ions (Leisner et al. 2006; Russell and Blanco-Cano 2007) when the distance between the Cassini spacecraft and Saturn is about 3.5–6.5 R_S (Cowee et al. 2009). After the neutral particles in the neutral cloud are ionized, they are accelerated in the direction perpendicular to the ambient magnetic field by Saturn's corotation electric field, a process called ion pickup. The pickup ions are created from the extended neutral cloud that encircles Saturn and are sourced by the moon Enceladus, orbiting at 3.95 Saturn radii (1 $R_S = 60{,}268$ km) (Leisner et al. 2006). The pickup ion gyrovelocity can be estimated from the difference between the neutral cloud velocity and the plasma corotation velocity as $v_{\perp 0} = v_{\text{corotate}} - v_{\text{neutral}}$. At the distance of Enceladus's orbit, $R = 3.95\ R_S$, the neutral cloud velocity is $v_{\text{neutral}} = \sqrt{GM/R} \approx 12.6$ km/s and the plasma corotation velocity is $v_{\text{corotate}} = R\Omega \approx 39$ km/s and thus $v_{\perp 0} \approx 26.4$ km/s. The pickup ions can form a ring velocity distribution in the direction perpendicular to the ambient magnetic field. This results in large temperature anisotropy, which is able to excite ICWs (Blanco-Cano 2004). Measurements by the Cassini plasma spectrometer (CAPS) showed that the velocity distributions of the W^+ ions are composed of both thermal ions (core) with a density $n_{\text{thermal}} = 33\ \text{cm}^{-3}$ and ring ions with a density $n_{\text{ring}} = 20.6\ \text{cm}^{-3}$ (which includes the density of the new pickup ion of 5.2 cm^{-3}). This is the case in the equatorial region in the distance range of 4–4.5 R_S (Tokar et al. 2008). When Cassini was close to the orbit of Enceladus, its magnetometer observed the magnetic field

*Correspondence: mchou@pssc.ncku.edu.tw
[1] Department of Physics, National Cheng Kung University, No. 1 University Road, Tainan 70101, Taiwan
Full list of author information is available at the end of the article

fluctuations with a magnitude increasing from 4% to 7% of B_0. The typical gyroradius of the newly picked up ions was about 10 km, while the gyrofrequency was about 0.3 Hz (Jia et al. 2010).

In this study, we analyze the distribution of ICWs from the Cassini MAG data for the period from January 2005 to December 2009. These data have a sampling time of 0.031 s, 0.062 s, 0.125 s, etc. and are presented in Kronographic (KRTP) coordinates, in which $\hat{r}$ points from Saturn to the spacecraft, $\hat{\varphi}$ is the unit vector of the azimuthal angle with respect to the magnetic axis, and the polar angle $\hat{\theta}$ completes the right-hand orthogonal coordinate. The 5-year magnetic field data for the ICW survey cover all local time sectors, and the statistical results provide the spatial distribution of ICWs in Saturn's inner magnetosphere. Most ICWs are found to be inside 6 R_S from Saturn for all local time sectors. However, the wave source region can also be outside of 6 R_S (and even extend beyond 7 R_S), though this mainly occurs in the midnight region. By examining four Cassini orbits that passed through the same location (radial distance and local time), Leisner et al. (2007) reported that the wave strength peaked away from the equator at about ± 0.25 R_S. However, in our study this phenomenon is also found to be local time dependent.

Data processing begins with frequency filtering near the gyrofrequency of W^+ (the water-group ions O^+, HO^+, H_2O^+ and H_3O^+), and the selected data are given in "Spatial distribution of W^+ gyrofrequency wave events" section. In section "Transverse and compressional waves," the variation of the $\delta B_\perp$ to $\delta B_{||}$ ratio for the ICWs with respect to the radial distance from Saturn is examined. The wave polarization when Cassini is located beyond 6 R_S is studied in section "Wave polarization," and the source region of ICWs is analyzed in section "Source region of ion cyclotron waves observed at high latitudes." In section "Ion cyclotron wave amplitude versus latitude", we present the statistical intensity distribution of ICW events in Saturn's magnetosphere. To explain the observations, we derive the local stability condition of ICWs based on kinetic theory, with pickup ions treated as a cold-ring distribution and background thermal ions treated as a Maxwellian distribution. This allows us to determine the local growth rate in section "Growth rate of ICW and its latitudinal dependence." Finally, the conclusions are given in section "Conclusion."

Spatial distribution of W^+ gyrofrequency wave events

A fast Fourier transform (FFT) is performed after the magnetic field data have been detrended. The selected bandwidth is ± 0.1 Hz with respect to the peak frequency. Signals with frequencies close to the local water-group ion cyclotron frequency f_{W+} (within 40%, in the spacecraft moving frame) are analyzed in this section. Then, for these selected data, the magnetic perturbations with dominant transverse components ($\delta B_\perp / \delta B_{||} > 2$) and left-hand polarization are identified as ICWs.

First, the Cassini spacecraft's orbits are projected in a Saturn-centered rectangular (X, Y, Z) coordinate system. This is defined with the X–Y plane being Saturn's equatorial plane, with the Z-axis along Saturn's magnetic axis, the Sun in the X–Z plane, and the positive Y-axis pointing toward the dusk. Note that we do not differentiate the rotational axis from the magnetic axis because their angles differ by less than 1°. We thus assume that they are in the Z-direction. Figure 1a–e shows a projection of the Cassini orbits in the X–Y plane in the left panels and the projection in the R–Z plane of the cylindrical coordinate in the right panels. This is plotted for each year from January 2005 to December 2009. The Cassini orbit is shown in red when the wave frequency obtained from the magnetic field data is near the local W^+ gyrofrequencies. The Cassini orbit projection in the X–Y equatorial plane (left panels) indicates the local time coverage. The orbit projection in the cylindrical R–Z plane (right panels) indicates the orbit inclination.

In the 2005 data (Fig. 1a), the W^+ cyclotron waves are detected in the noon, dusk and midnight regions, with the magnetic latitude θ between $-10°$ and 8° and the radial distance R between 3.5 R_S and 7.8 R_S. In the 2006 data (Fig. 1b), the W^+ cyclotron waves are detected mostly in the noon and dusk sectors, with θ between $-7°$ and 7° and R between 4 R_S and 7.5 R_S. In the 2007 data (Fig. 1c), the W^+ cyclotron waves are detected in the midnight and dawn regions, with θ between $-8°$ and 20° and R between 3.6 R_S and 7.2 R_S. In the 2008 data (Fig. 1d), wave signals are found in the midnight region with $\theta \sim -40°$–30° and $R \sim$ 3.7–6 R_S. In the 2009 data (Fig. 1e), the W^+ cyclotron waves are detected in the midnight, dawn and noon regions with θ between $-12°$ and 18° and R between 3.6 R_S and 7.7 R_S. The 5 years of data show that most of the ICW signals are found inside $\theta \sim \pm 5°$ except for the 2008 data and part of the 2007 data, when Cassini was in the midnight sector. The latitudinal and local time dependence of ICWs will be further discussed in section "Ion cyclotron wave amplitude versus latitude."

Transverse and compressional waves

The ratio of $\delta B_\perp$ to $\delta B_{||}$ helps to determine the wave type, where the subscripts $\perp$ and $||$ indicate the components perpendicular and parallel to the ambient magnetic field, respectively. If $\delta B_\perp / \delta B_{||}$ is larger (smaller) than one, the magnetic fluctuations can be regarded as transverse (compressional) waves. To obtain the magnetic field perturbations in the perpendicular and parallel directions to the ambient magnetic field, the KRTP coordinates are

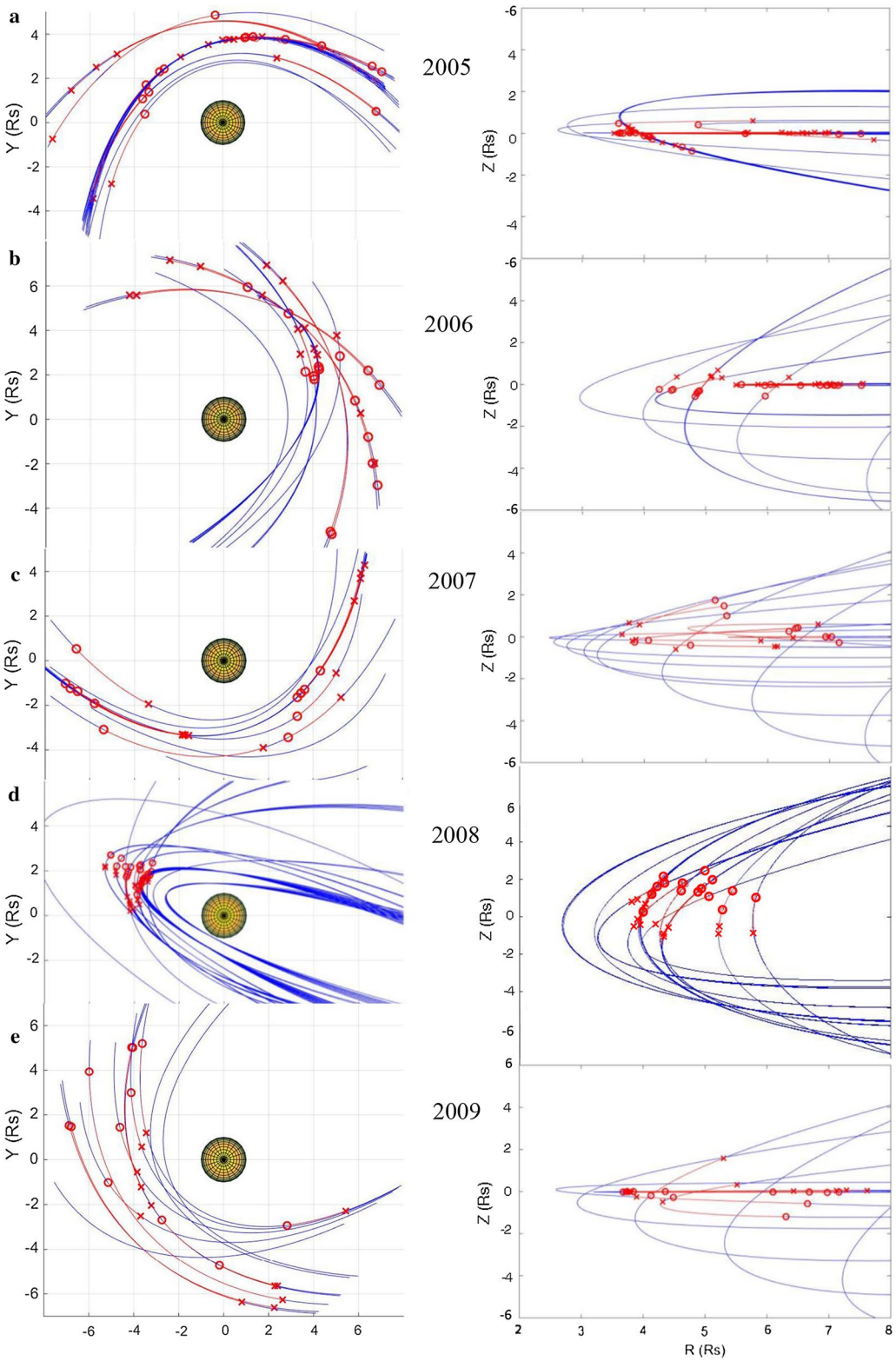

Fig. 1 **a** Cassini orbit projection in the *X*–*Y* equatorial plane, in a Saturn-centered coordinate system. **b** Cassini orbit projection in the cylindrical *R*–*Z* plane. The positive *X*-axis is pointing toward noon time. The orbit curves are in *red* when the wave frequencies are near to the local water-group ion gyrofrequencies

locally rotated such that $\hat{\theta}$ aligns with the ambient magnetic field direction. The averaged value of $\delta B_\perp$ is calculated by $\delta B_\perp = \left\langle \sqrt{(\delta B_r)^2 + (\delta B_\varphi)^2} \right\rangle$, where the bracket means the average over a time period much longer than the wave period or an orbital distance. For example, the data series in the form $\delta B_\phi = \sin(\omega t)$ and $\delta B_r = \cos(\omega t)$ results in $\delta B_\perp = 1$.

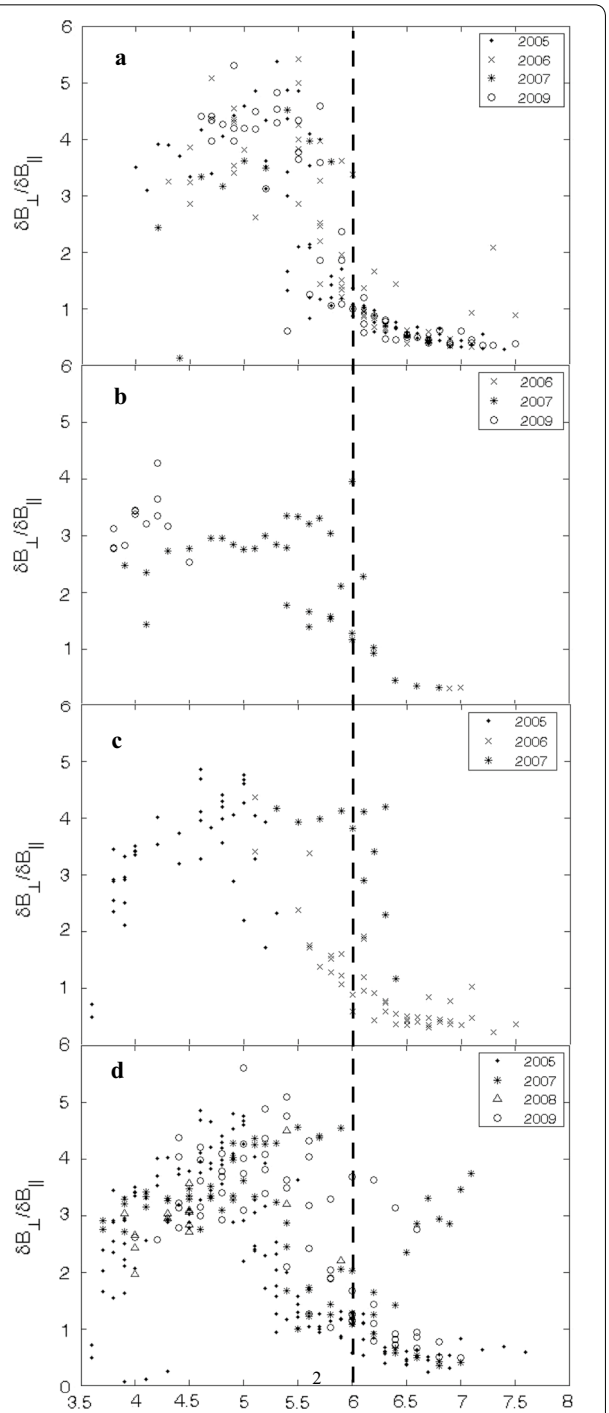

Fig. 2 $\delta B_\perp/\delta B_{||}$ versus the Cassini cylindrical radial distance R in the low-latitude (±5°) region for **a** noon, **b** dawn, **c** dusk and **d** midnight sectors. *Each dot* represents the averaged value within a radial distance of $\Delta R = 0.2\ R_S$ for each event

The average value of $\delta B_{||}$ is calculated by $\delta B_{||} = \sqrt{2\langle(\delta B_\theta)^2\rangle}$, where the average bracket value is multiplied by 2 inside the square root to give the correct wave amplitude for a sinusoidal wave. Figure 2 shows the ratio of $\delta B_\perp$ to $\delta B_{||}$ versus the cylindrical radial distance R, in the low-latitude (±5°) region. The results for the noon, dawn, dusk and midnight sectors are shown in panels (a), (b), (c) and (d), respectively. For each data point, $\delta B_\perp$ and $\delta B_{||}$ are averaged over an orbital distance with $\Delta R = 0.2$ R_S each time Cassini passes through the waves.

These 5 years of data have the same characteristics: Transverse waves are mostly inside 6 R_S. The data points with $\delta B_\perp/\delta B_{||} \gg 1$ outside 6 R_S are mainly in the midnight sector (see Fig. 2d). Some data points with $\delta B_\perp/\delta B_{||} \gg 1$ outside 6 R_S also occur in the dusk sector (see 2007 data points in Fig. 2c) although they are found at the very edge of the dusk sector and close to the midnight sector. The data points with small $\delta B_\perp/\delta B_{||}$ values represent compressional-type waves. The data points with large $\delta B_\perp/\delta B_{||}$ values are identified as ICWs if they have left-hand polarization. Some examples of ICW events are given in the next section.

Wave polarization

In the analysis of the dayside and nightside segments of Rev. 19, Russell et al. (2006) reported that mirror modes can emerge outside 5 R_S and that ICWs appear inside 7 R_S. This is in general agreement with the analysis results from the five-year data, covering all local time sectors. For $R < 6$ R_S, we found that waves at low latitudes are mostly left-hand circularly polarized. They are identified as ion cyclotron waves. For $R > 6$ R_S, waves are generally in a compressional mode (though some mixed polarization cases can be found, see "Waves with mixed polarization" section), but waves near the midnight region are transverse, left-hand circularly polarized.

Left-hand circularly polarized waves: ion cyclotron waves

Figure 3 shows a typical left-hand circularly polarized wave event for $R < 6$ R_S. The perturbed magnetic field components in KRTP coordinates are shown in Fig. 3a, for a time interval of 3 min during 00:50 to 00:53 UT on July 24, 2006. The perturbed magnetic field components are filtered with a band width of ±0.08 Hz with respect to the peak frequency, and the distance between Cassini and Saturn is 4.7 R_S; the latitude is −1°; the background magnetic field mean value is ~200 nT; and the observed wave frequency is ~0.17 Hz (f_{O^+} is ~0.19 Hz). Figure 3b shows

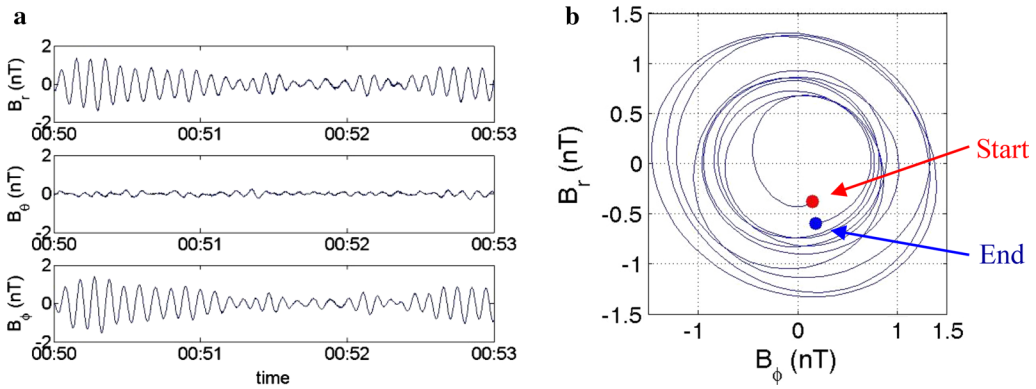

Fig. 3 An ion cyclotron wave event for $R < 6\ R_S$ on July 24, 2006. **a** Perturbed magnetic field in the KRTP coordinates, B_0 ~200 nT, and **b** the wave polarization. The *red point* denotes the start time and the *blue point* denotes the end time

left-hand polarization for the perturbed magnetic field. We can estimate the wavelength and the phase velocity of the ion cyclotron waves by assuming that they propagate mainly along the ambient magnetic field line in the low-latitude equatorial region. The observed Doppler shift frequency can be written as $\omega' \approx \omega - k_\theta v_{s\theta}$, where $v_{s\theta}$ is the spacecraft velocity in the θ direction. For the case shown in Fig. 3, $\omega' = 1.05$ rad/s and $v_{s\theta} = -3.77$ km/s. If the ion cyclotron wave frequency is the same as the O^+ gyrofrequency (given by $\omega = 1.23$ rad/s) in the plasma moving frame, then $k_\theta \approx (\omega - \omega')/v_{S\theta} = -0.033\ \text{km}^{-1}$ (the wavelength is $\lambda = 2\pi/|k_\theta| = 188.7$ km) and the phase velocity in the θ direction is $V_{\text{ph}} = \omega/k_\theta = -36.2$ km/s (i.e., northward propagation). Note that our calculation is for a single event, which is different from the statistical average over different events performed by Leisner et al. (2011).

Figure 4 shows an ion cyclotron wave event for $R > 6\ R_S$ in the low-latitude region. The perturbed magnetic field components in KRTP coordinates are shown in Fig. 4a, for a time interval of 3 min during 02:45 to 02:48 UT on September 30, 2007. The left-hand circular polarization for the perturbed magnetic fields is shown in Fig. 4b. The perturbed magnetic field components are filtered with a band width of ±0.02 Hz, with respect to the peak frequency, and the distance between Cassini and Saturn is 7.1 R_S; the latitude is −2°; the longitude is 147.6° with respect to the X-axis (counterclockwise, in the midnight region); the background magnetic field mean value is 50 nT; and the observed wave frequency is ~0.039 Hz, which is about 20% below the O^+ cyclotron frequency f_{O^+} of ~0.047 Hz. Thus, based on the wave frequency, the dominant transverse perturbation and left-hand circular polarization of the ICWs are identified inside 6 R_S at all local times. For ICW events outside 6 R_S, 42% of events with a frequency close to f_{W+} were identified as ICWs in the 2007 data (with Cassini orbits ranged from pre-midnight to dawn). 7% were identified in the 2009 data (with Cassini orbits ranging from midnight to noon), and all the detected ICWs were near the midnight region.

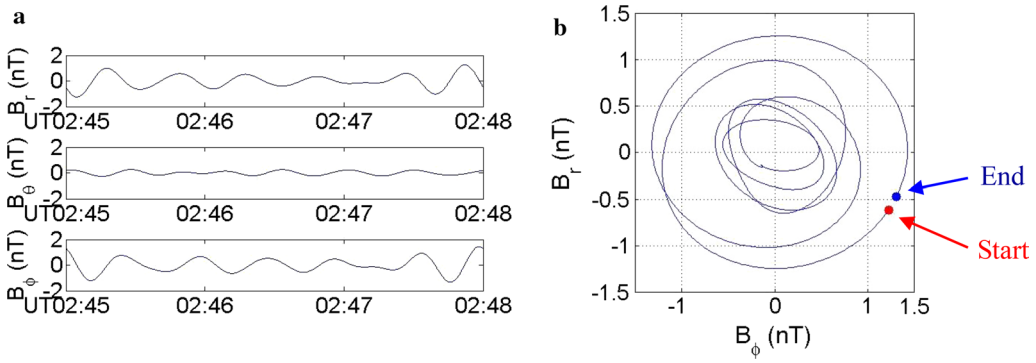

Fig. 4 An ion cyclotron wave event for $R > 6\ R_S$ on September 30, 2007. **a** Perturbed magnetic field components in the KRTP coordinates, B_0 ~50 nT, and **b** the left-hand circular polarization of the magnetic field components. The *red point* denotes the start time and the *blue point* denotes the end time

Waves with mixed polarization

A typical wave event with a mixed polarization, outside 6 R_S in the low latitudes, is shown in Fig. 5. Figure 5a shows the perturbed magnetic field for a time interval of 3 min during 20:53 to 20:56 UT on October 13, 2009. The distance between Cassini and Saturn is 6.3 R_S; the latitude is −0.308°; and the background magnetic field mean value is ~58 nT. Figure 5b shows the left-hand circular polarization in the wave's transverse components (δB_r and δB_ϕ) with a frequency of 0.04 Hz which is about 25% below the O^+ cyclotron frequency (f_{O^+} of 0.05 Hz). Figure 5c shows a mixture of linear and left-hand circular polarizations in δB_θ and δB_ϕ. However, from Fig. 5a the dominant frequency of δB_θ can be seen to be about a factor of 2 smaller than that of the transverse components. Thus, the magnetic perturbations are considered to be a linear superposition of the compressional mirror mode (Cowee et al. 2009) and transverse ion cyclotron waves.

Linearly polarized waves: mirror modes

A typical compressional wave event, with linear polarization outside 6 R_S in the low-latitude region, is shown in Fig. 6. Figure 6a shows the perturbed magnetic field for a time interval of 20 min during the period from 02:20 to 02:40 UT on March 9, 2005, when Cassini was 7 R_S from Saturn and its latitude was −0.2°. The amplitude of the δB_θ component, which is mainly along the ambient magnetic field, is much larger than the amplitudes of the other two perturbed magnetic field components. Thus, the wave is of a compressional type and has a linear polarization as shown in Fig. 6b. The observed wave frequency (0.01 Hz) is much smaller than the O^+ cyclotron frequency, which is f_{O^+} of 0.045 Hz for the background magnetic field with a mean value of 48 nT. Thus, the wave event is considered as a mirror mode due to its compressional nature and characteristic waveform (Russell and Blanco-Cano 2007).

Based on the magnetohydrodynamics (MHD) theory, the mirror mode is stationary (with zero frequency) in the plasma moving frame. However, when particle kinetic effects are considered, the mirror mode has a small real frequency associated with the diamagnetic drift frequency of the plasma density gradient (Hasegawa 1969). If the plasma is moving, it will also move with the plasma (e.g., Johnson and Cheng 1997). Thus, the Doppler

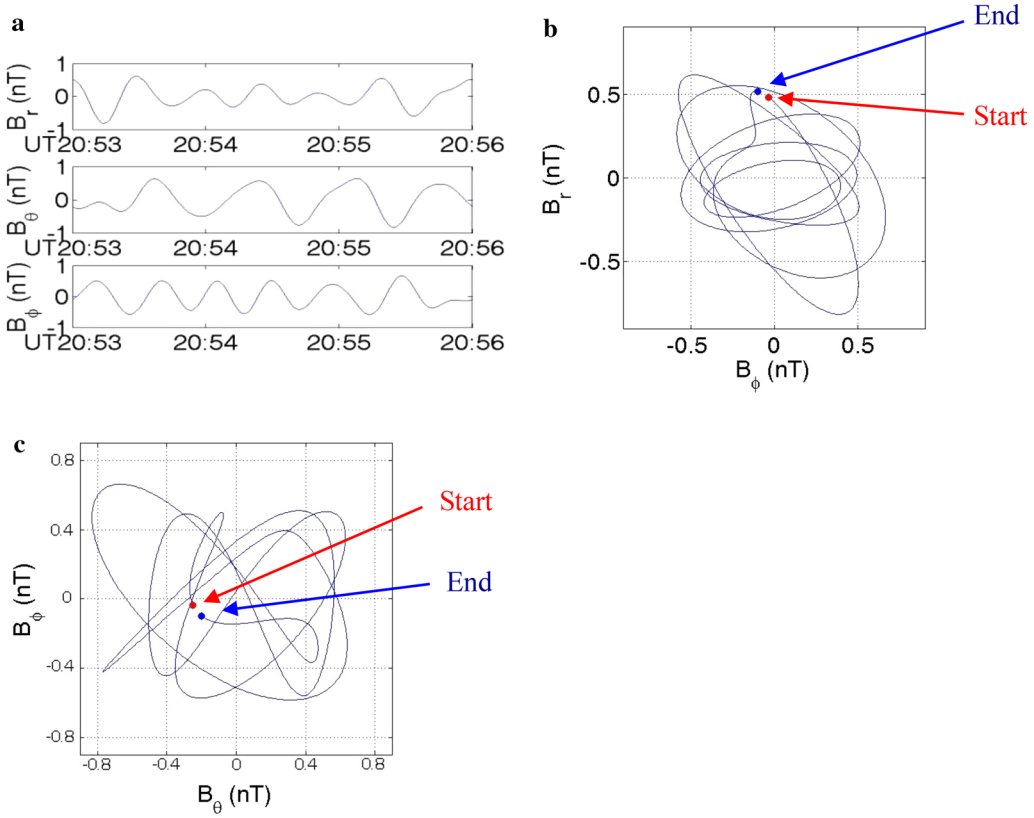

Fig. 5 An event showing the superposition of a transverse ion cyclotron wave and a compressional mirror mode for *R* outside 6 R_S on October 13, 2009. **a** Perturbed magnetic field components in KRTP coordinates, B_0 ~58 nT, and **b** *left-hand circular* polarization in the transverse magnetic components. **c** The mixture of the parallel compressional mirror mode and the transverse ICW magnetic components. The *red point* denotes the start time and the *blue point* denotes the end time

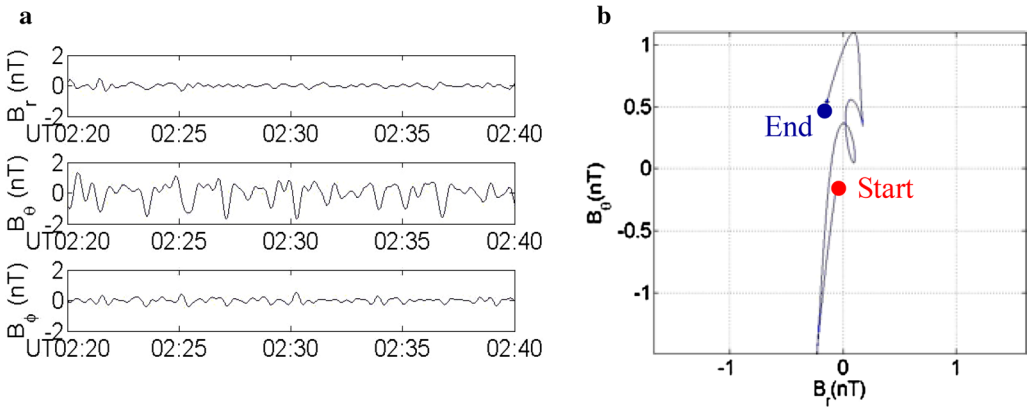

Fig. 6 A mirror-mode event for R outside 6 R_S on March 9, 2005. **a** Perturbed magnetic field components in the KRTP coordinates, B_0 ~48 nT, and **b** the linear polarization in δB_θ. The *red point* denotes the start time and the *blue point* denotes the end time

frequency shift is caused by both the plasma flow velocity and the satellite moving velocity. For mirror modes, we assume that the wave vector is mainly perpendicular to the ambient magnetic field. The plasma flow is dominated by both the corotation velocity (v_{cor} ~39 km/s at Enceladus orbit), which is mainly in the azimuthal direction and is much larger than the satellite velocity (v_s ~10 km/s), as well as the radial flow velocity (up to 2 km/s, Wilson et al. 2008). This means that the Doppler shift frequency is given by $\omega' \approx k_\varphi v_{\rm cor} + k_\varphi v_{s\varphi} + k_r v_{sr}$, where $v_{s\varphi}$ and v_{sr} are the spacecraft velocity in the φ-direction and r-direction, respectively. The mirror-mode free energy is associated with anisotropy in the pickup ion velocity space and is localized in the r-direction but is much broader in the φ-direction. This means that the wave vector is assumed to be mainly in the r-direction in order to carry the wave energy out of the unstable region for saturation. Thus, $k_r \gg k_\varphi$, and the Doppler shift is caused mainly by the satellite velocity and is given by $\omega' \approx k_r v_{sr}$. For the mirror mode shown in Fig. 6, the Doppler shift frequency is $\omega' \approx k_r v_{sr} = 0.01$ rad/s, and for $v_{sr} = 10$ km/s, we obtain a value for $k_r = 10^{-3}$ km^{-1}, and the radial wavelength $\lambda = 2\pi/k_r = 6283.2$ km.

Source region of ion cyclotron waves observed at high latitudes

In comparison with other years, the Cassini orbits in 2008 are more often in the high-latitude region of the inner magnetosphere. The upper panel of Fig. 7 shows a Cassini orbit (the red line) moving across the L-shell field lines from the northern high-latitude region (A) to the southern high-latitude region (B). The lower panel of Fig. 7 shows the power spectrum of δB for an ion cyclotron wave event observed on August 4, 2008, and Cassini passes from point A ($r = 4.26$; $\theta = 27.3$) in the Northern Hemisphere to point B ($r = 4.23$; $\theta = -40.7$) in the Southern Hemisphere, where r is the radial distance of Cassini from Saturn in a spherical coordinate system and θ is the magnetic latitude. The blue dashed line shows the local W^+ gyrofrequencies $f_{\rm local}$, and the black line shows the W^+ gyrofrequency $f_{\rm eq}$ at the dipole L-shell equator of the Cassini orbit field lines. To calculate $f_{\rm eq}$, we assume that in Saturn's inner magnetosphere the magnetic field can be well described by the dipole field model. The dipole field line is determined by $r = LR_s \cos^2\theta$, where L is the L-shell value. The dipole magnetic field at the equator is given by $B_{eq} = B_0/L^3$, where $B_0 = 2 \times 10^4$ nT is the magnetic field strength at the equator on Saturn's surface. The corresponding equatorial gyrofrequency for the L-shell field line going through point A is $f_{\rm eqA} = 0.095$ Hz for $L = 4.26/\cos^2(27.3°) = 5.4$, and the equatorial magnetic field strength is $B_{\rm eqA} = B_0(5.4)^{-3} = 10$ nT. Similarly, the corresponding equatorial W^+ gyrofrequency for the $L = 7.4$ field line going through point B is $f_{\rm eqB} = 0.0475$ Hz and the equatorial magnetic field strength is $B_{\rm eqB} = 50$ nT.

From the lower panel of Fig. 7, we note that the observed wave frequencies are lower than the local W^+ gyrofrequency (blue dotted line), except near the equator, and in the higher-latitude region where they are at least two times smaller than the local W^+ gyrofrequency. However, the observed wave frequency matches well with the calculated equatorial W^+ gyrofrequency $f_{\rm eq}$ (black line) of the corresponding L-shell field line. This supports the postulation that the ion cyclotron waves observed in the high-latitude region have their source farther away in the low-latitude equatorial region, from which the ion cyclotron waves propagate along magnetic field lines to the higher-latitude region. Note that this is also consistent with the Doppler shift analysis done by Leisner et al.

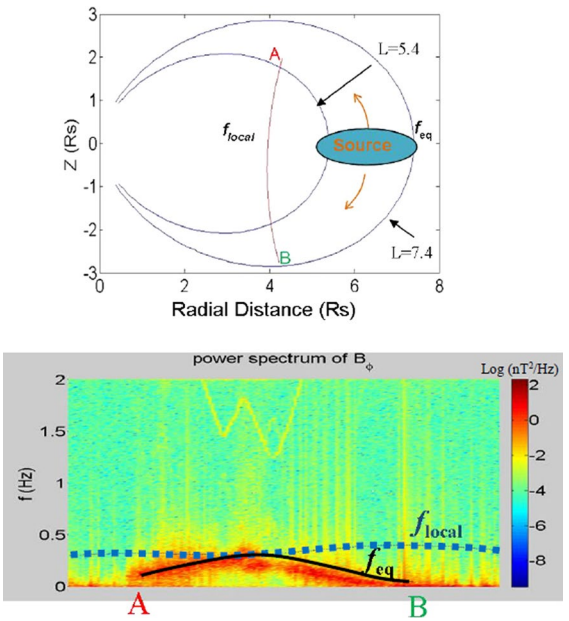

Fig. 7 The *upper panel* shows the projected orbit of Cassini in the cylindrical *R–Z* plane across the *L*-shell from the Northern Hemisphere to the Southern Hemisphere. The *red line* denotes Cassini's orbit and the *blue lines* denote the *L*-shell field lines going through *points A* and *B*, respectively. The *lower panel* shows the power spectrum of δB_ϕ, the *blue dotted line* shows the local W^+ gyrofrequency (f_{local}), and the black line is the W^+ gyrofrequency at the equator (f_{eq}) of the dipole *L*-shell of the Cassini orbit, which moves from *A* to *B*

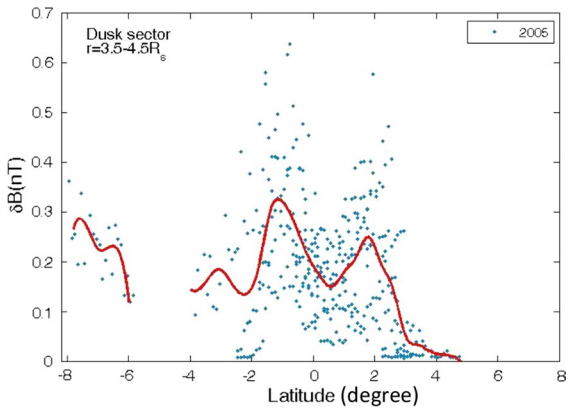

Fig. 8 The averaged perturbed magnetic field amplitude δB in the radial distance range of 3.5–4.5 R_S versus latitude for the dusk sector collected from the 2005 data. *Each point* represents the averaged δB within a small region of $\Delta\theta = 0.1°$ and $\Delta R = 1\ R_s$ when Cassini passed through

(2011) on the 2006 MAG data and the hybrid simulation near Enceladus' orbit done by Cowee et al. (2009). The wave sources are near the equator, and the waves then propagate both northward and southward along the field lines to the high-latitude regions. However, Cassini moves southward, and thus, the observed wave frequency is downward shifted in the Southern Hemisphere as opposed to an upward frequency shift in the Northern Hemisphere.

Ion cyclotron wave amplitude versus latitude

In order to determine how the ICW amplitude depends on latitude, we plot the averaged δB versus latitude for different radial distance regions, using data selected from that in "Spatial distribution of W^+ gyrofrequency wave events" section, where

$$\delta B = \left\langle \sqrt{(\delta B_r)^2 + (\delta B_\theta)^2 + (\delta B_\varphi)^2} \right\rangle \quad (1)$$

The magnetic components are obtained by a band-pass filter with a bandwidth of ±0.1 Hz with respect to the peak frequencies. Each point for δB shown in Figs. 8, 9 and 10 is averaged within a small region of the magnetic latitude range $\Delta\theta = 0.1°$ with an equatorial radial distance range of $\Delta R = 1\ Rs$ when Cassini passed through.

Figure 8 plots the 2005 data. It shows the latitude dependence of the perturbed magnetic field amplitude δB, averaged at a radial distance range of 3.5–4.5 R_S in the dusk sector. The average δB amplitude versus the latitude is shown by the red curve, and it is clear that the peaks of δB are off the equator with maxima at about 1.8° and −1.2° latitude in the dusk sector.

Figure 9 plots data collected from 2005, 2006, 2007 and 2009. It shows the latitude dependence of the perturbed magnetic field amplitude δB averaged over the data at a radial distance range of 4.5–5.5 R_S for the noon sector. The black circles represent δB values on July 26, 2009, only, and the pink dots represent 2009 data without the data for July 26, 2009. In general, the off-equator peaks are found to be at about 2° and −2° latitude in the noon sector. However, the off-equator peak became broader and moved radically to about 10° on July 26, 2009.

Figure 10 plots data collected from 2006, 2007, 2008 and 2009. It shows the latitude dependence of the perturbed magnetic field amplitude δB averaged over the data in the radial distance ranges of (a) 3.5–4.5 R_S, (b) 4.5–5.5 R_S and (c) 5.5–6.5 R_S for the midnight sector. The average δB amplitude versus latitude is shown by the red curve. The peak of the average wave amplitude increases with increasing distance from Saturn. In Panel (a), the average δB peaks are at 4° and −3.5° latitude, with an average δB of ~0.7 nT. In Panel (b), the average δB peaks are at 4.5° and −3° latitude with an average δB of ~1.2 nT. In Panel (c), the average δB peaks are at 5° and −4° latitude with an average δB of ~1.7 nT. For the dawn sector, however, Cassini had no good latitudinal coverage from which to draw conclusions.

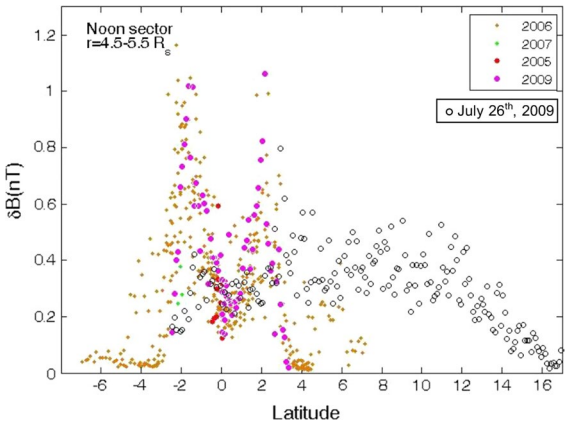

Fig. 9 The latitude dependence of the averaged perturbed magnetic field amplitude δB in the radial distance range of 4.5–5.5 R_S for the noon sector for the data from 2005, 2006, 2007 and 2009. *Each point* represents the averaged δB within a small region of $\Delta\theta = 0.1°$ and $\Delta R = 1\ R_s$ when Cassini passed through. It is noted that the latitude distribution of δB on July 26, 2009, peaked at ~10° which is different from the other data that show the δB peaks are at +2° and −2°

From Figs. 8, 9 and 10, the latitude position of maximum δB can be seen to be at a higher latitude in the midnight sector. It generally moves to a lower latitude in the noon sector and an even lower one in the dusk sector. Also, the latitudinal width of the δB peaks (the average δB intensity is shown by the red lines) is found to be broader in the midnight sector and becomes narrower in the noon and dusk sectors.

Figure 11 shows a projection of the δB intensity distribution in the equatorial plane (in rectangular X–Y coordinates) for the data from 2005 to 2009. The data are selected in between ±1° latitude from the magnetic equator to avoid the latitudinal effect. The ICW amplitude is relatively large in this region between the midnight and dawn, and the maximum amplitude occurs in the midnight region.

Growth rate of ICW and its latitudinal dependence

To understand why the maximum ICW wave amplitude is located off the equator, we investigate the stability of the left-hand circularly polarized ion cyclotron wave based on kinetic theory. The W^+ ion is assumed to be composed of two distributions: Firstly, the cold-ring velocity distribution $f_{i0} = 1/(2\pi v_{\perp 0})\delta(v_\perp - v_{\perp 0})\delta(v_{||})$ for the pickup ions, which are responsible for destabilizing the ion cyclotron waves. Secondly, the background plasma has an isotropic Maxwellian distribution with temperature T, which contributes to the wave stabilization. The H^+ component becomes important at high latitude, but we concentrate our discussion on the low-latitude equatorial region. Then, based on linear kinetic theory the local dispersion relation for the left-hand polarized waves can be written as:

$$\omega^2 = k_{||}^2 c^2 + \omega_{\rm pr}^2 \left[\frac{\omega}{\omega - \omega_c} + \frac{k_{||}^2 v_{\perp 0}^2}{2(\omega - \omega_c)^2} \right] - \frac{\omega_{\rm pi}^2 \omega}{k_{||} v_{\rm th}} Z(\zeta) \tag{2}$$

where $\omega_{\rm pr}$ and $\omega_{\rm pi}$ are the plasma frequency of the ring and thermal components, respectively. ω_c is the ion gyrofrequency and $v_{\rm th}$ is the thermal speed of the thermal component. Z is the plasma dispersion function with the argument $\zeta = (\omega - \omega_c)/k_{||} v_{\rm th}$. The pickup ion gyrovelocity can be estimated from the difference between the neutral cloud velocity and the plasma corotation velocity as $v_{\perp 0} = v_{\rm corotate} - v_{\rm neutral}$. At the distance of Enceladus' orbit ($R = 3.95\ R_S$), the neutral cloud velocity is $v_{\rm neutral} = \sqrt{GM/R} \approx 12.6$ km/s, the plasma corotation velocity is $v_{\rm corotate} = R\Omega \approx 39$ km/s, and thus, $v_{\perp 0} \approx 26.4$km/s. In Eq. (2), the second term represents the ring particle contribution and the third term is contributed by the thermal ions. Let $X \equiv (\omega - \omega_c)/\omega_c$ and assume $|X| \ll 1$ and $|\zeta| >> 1$, then Eq. (2) can be simplified to

$$\left[1 + \frac{k_{||}^2 c^2}{\omega_{\rm ptot}^2} - \frac{\omega_c^2}{\omega_{\rm ptot}^2} \right] X^2 + X + \left(\frac{n_{\rm ring}}{n_{\rm tot}} \right) \frac{k_{||}^2 v_{\perp 0}^2}{2\omega_c^2} \cong 0 \tag{3}$$

by dropping the higher order terms, where $\omega_{\rm ptot}$ is the total plasma frequency associated with the total ion density $n_{\rm tot} \equiv n_{\rm ring} + n_{\rm thermal}$. For a typical pickup W^+ ion density of n_i~ O(10) $\rm cm^{-3}$ with the equatorial magnetic field intensity of B ~(20,000/L^3) nT, we have $\omega_c^2 << \omega_{ptot}^2$, and the solution of Eq. (3) is given by:

$$\frac{\omega}{\omega_c} \cong 1 - \frac{1}{2(1 + k_{||}^2 c^2/\omega_{\rm ptot}^2)} \pm i \frac{\sqrt{2(n_{\rm ring}/n_{\rm tot})(k_{||}^2 v_{\perp 0}^2/\omega_c^2)(1 + k_{||}^2 c^2/\omega_{\rm ptot}^2) - 1}}{2(1 + k_{||}^2 c^2/\omega_{\rm ptot}^2)} \tag{4}$$

The condition for an unstable ICWs is then $2(n_{\rm ring}/n_{\rm tot})(k_{||}^2 v_{\perp 0}^2/\omega_c^2)(1 + k_{||}^2 c^2/\omega_{\rm ptot}^2) > 1$, and the growth rate is expressed as:

$$\frac{\gamma}{\omega_c} \cong \frac{\sqrt{2(n_{\rm ring}/n_{tot})(k_{||}^2 v_{\perp 0}^2/\omega_c^2)(1 + k_{||}^2 c^2 m_i/4\pi n_{\rm tot} e^2) - 1}}{2(1 + k_{||}^2 c^2 m_i/4\pi n_{\rm tot} e^2)} \tag{5}$$

Note that the growth rate increases with increasing $v_{\perp 0}$ and $n_{\rm ring}$. For a fixed ratio of $n_{\rm thermal}/n_{\rm ring} = R_n$, from Eq. (5), the ICW is unstable for $n_{tot} < k_{||}^2 c^2 m_i/4\pi e^2 [(1+R_n)\omega_c^2/2 k_{||}^2 v_{\perp 0}^2 - 1]$.

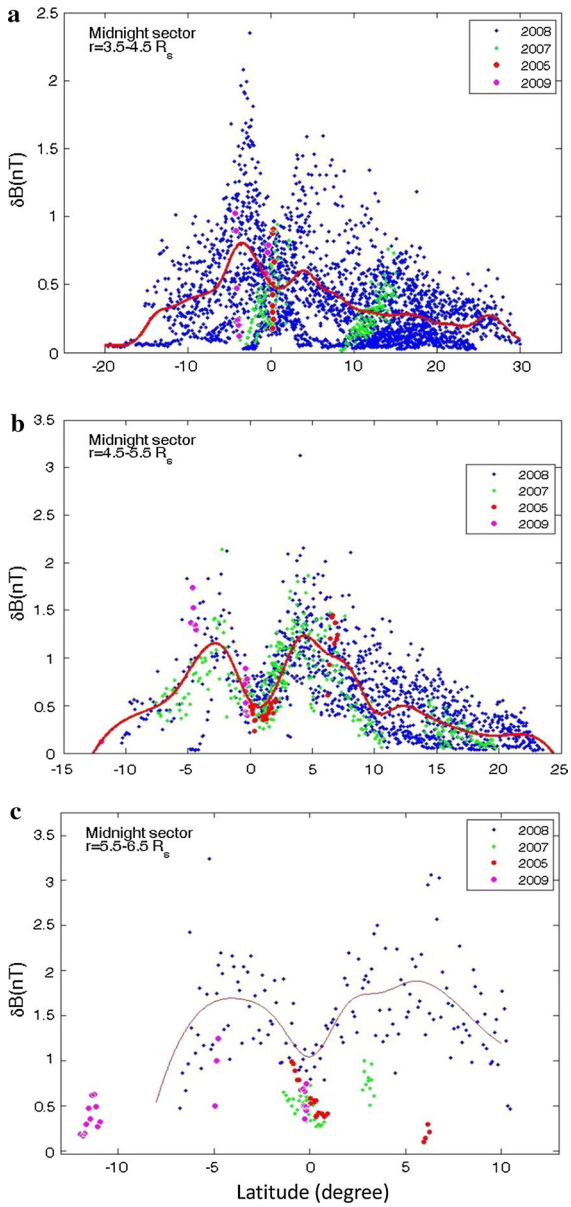

Fig. 10 The latitude dependence of the averaged perturbed magnetic field amplitude δB in the radial distance range of **a** 3.5–4.5 R_S, **b** 4.5–5.5 R_S and **c** 5.5–6.5 R_S for the midnight sector for the data from 2005, 2007, 2008 and 2009. *Each point* represents the averaged δB within a small region of $\Delta\theta = 0.1°$ and $\Delta R = 1$ R_s when Cassini passed through

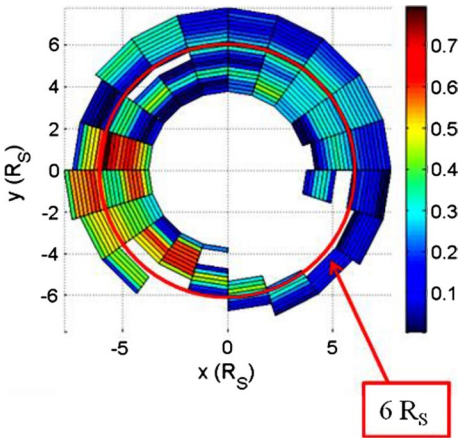

Fig. 11 The projection of the ICW δB amplitude distribution in the equatorial plane in a rectangular *X*–*Y* coordinate system, with the wave amplitude averaged over small areas of $\Delta R = 0.5$ R_S and $\Delta_\varphi = 15°$ in a cylindrical coordinate system. The data were selected between ±1° latitude to avoid the latitudinal effect

Because the total plasma density decreases along the field line away from the equator, due to the plasma rotation effect, the growth rate will vary along the field line. As the total ion density n_{tot} decreases to $n_0 = k_{||}^2 c^2 m_i / 4\pi e^2 [(1+R_n)\omega_c^2 / k_{||}^2 v_{\perp 0}^2 - 1]$, the growth rate increases and reaches the maximum value given by $\gamma_{hboxmax}/\omega_c = k_{||}^2 v_{\perp 0|^2}/2(R_n+1)\omega_c^2$. When the total ion density n_{tot} decreases further with $n_{\rm tot} < n_0$, the growth rate starts to decrease. These analytical results are verified by the numerical solutions of Eq. (2).

To obtain numerical solutions of the dispersion relation (Eq. (2)) along the field lines, the B field in the inner magnetosphere of Saturn is approximated as a dipole field. The total ion density variation along the field lines is estimated from the 2D axisymmetric MHD force-balanced equilibrium model for azimuthally rotating plasmas, with small anisotropy of the total pressure (e.g., Chou and Cheng 2010). This is written as $n_W = n_{\rm eq} \exp[-m_i \Omega^2 (R_{\rm eq}^2 - R^2)/2T_{||}]$ due to the centrifugal force. $n_{\rm eq}$ is the equatorial ion density, Ω is the plasma rotation frequency, $T|$ is the ion temperature along the field line, $R_{\rm eq} = LR_S$ is the dipole L-shell distance, and R is the equatorial distance of the field line position. Tokar et al. (2008) reported that $n_{\rm thermal} = 33$ cm^{-3} and the density of the pickup ions is $n_{\rm ring} = 20.6$ cm^{-3} around $R = 4 - 4.5 R_S$ in the equatorial region (on October 11, 2005, from 21:08:03 to 22:06:43 UT) though these values are for a specific time. We set the density ratio as $R_n = n_{\rm thermal}/n_{\rm ring} = 3/2$ at the equator and calculated the R_n variation along B in order to study the growth rate. Figure 12a shows the dependence of growth rate on latitude along the $L = 4.5$ field line for different values of $k_{||}$, where the equatorial density is $n_{\rm eq} = 50$ cm^{-3} and the plasma rotation frequency is $\Omega = 1.64 \times 10^{-4}$/s.

The ion density along the $L = 4.5$ field line is concentrated at the equator as shown in Fig. 12b, due to the plasma rotation in Saturn's magnetosphere. The damping effect becomes strong around the equator and results in a local growth rate minimum at the equator. This

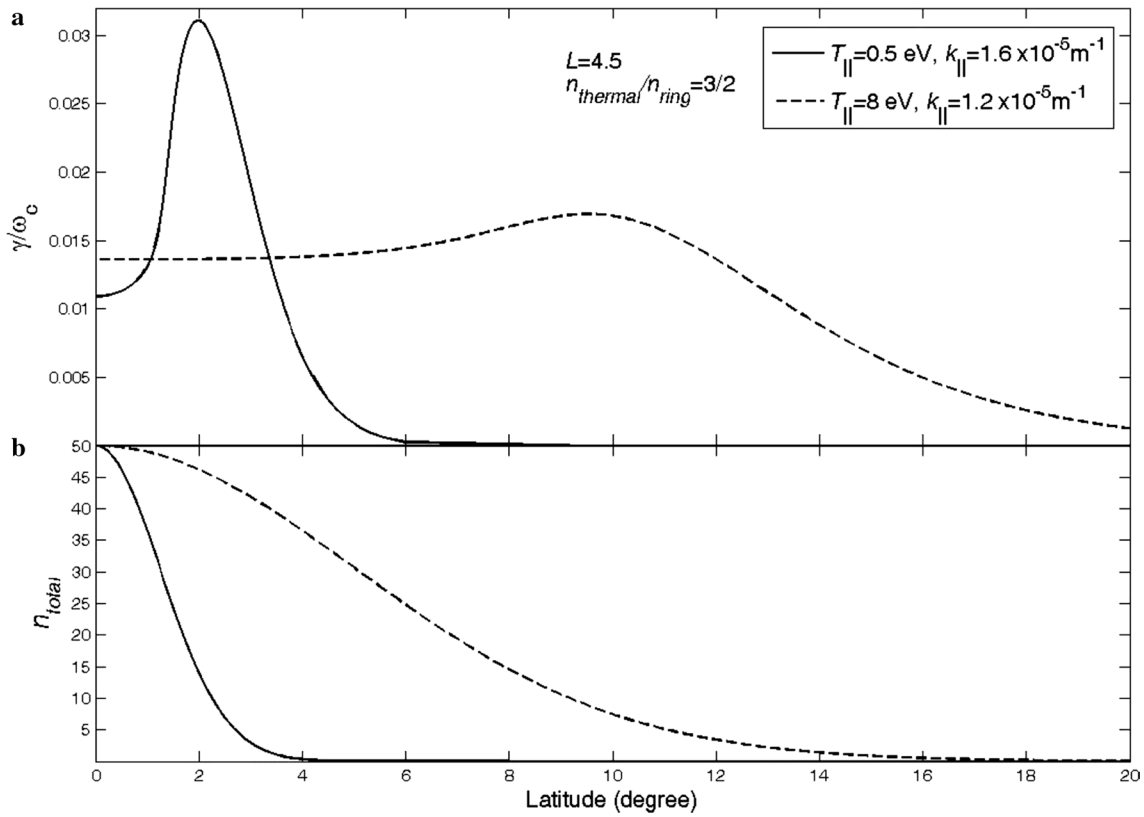

Fig. 12 **a** The dependence of ICW growth rate on latitude along the $L = 4.5$ field line for different wave number $k|$ and parallel ion temperature $T|$ values with these fixed parameters: the equatorial density $n_{eq} = 50\ cm^{-3}$, the plasma rotation frequency $\Omega = 1.64 \times 10^{-4}/s, v_{\perp 0} = 26.4$ km/s and the density ratio $R_n = n_{thermal}/n_{ring} = 3/2$. **b** The corresponding ion density versus the magnetic latitude along the $L = 4.5$ field *line*

gives a reasonable explanation for the observed latitudinal dependence of the ICW amplitude δB, as shown in Figs. 8, 9 and 10, such that the ICW amplitude has a local minimum at the equator. The maximum growth rate $\gamma_{\max}/\omega_c$ is sensitive to $k_{||}$ as shown in the analytical results (Eq. (5)). The latitudinal position of the peak growth rate (or the corresponding latitude at which $n_{tot} = n_0$) is sensitive to $T_{||}$ because the ion density variation scale length depends on $\sqrt{2T_{||}/m_i\Omega^2}$ in the Gaussian density model. By tuning $k_{||}$ and $T_{||}$, the latitudes of peak growth rate can be located at 2° and 10°. This is shown in Fig. 12a as a comparison to the observed δB peak in the noon sector (Fig. 9). The model implies that a higher temperature causes the off-equator growth rate peak to move to higher latitudes, which can explain the July 26, 2009, data. Thus, there could be a sudden increase in the plasma temperature on that day, and one possibility for the phenomena is that they occurred when Cassini was immersed in an energetic neutral atom (ENA) event.

The location of the peak growth rate moves to higher latitude for larger $T_{||}$ values, due to the broader density profiles along the field line. This can be used to infer the parallel temperature distribution over the local time, by comparing the latitudinal distribution of ICW amplitude with the observational data over the different local time sectors (as given in "Ion cyclotron wave amplitude versus latitude" section). The peak ICW amplitude is located at about ±4° for the midnight sector, about ±2° for the noon sector and about ±1.5° for the dusk sector. Because of this, and the trend of the δB peak width, we propose that the averaged parallel ion temperature decreases from a few eVs in the midnight sector, to lower values toward the dawn sector. This decrease continues through the noon sector and then drops to below ~1 eV in the dusk sector (although there was no good latitudinal coverage of data for the dawn sector from 2005 to 2009). The decrement in temperature implies that there are extra ICW driving sources on the nightside, in addition to the pickup ion mechanism near Enceladus' orbit.

Our local stability analysis of ICWs provides their local growth rate for each point along the field line. Ideally a nonlocal stability analysis along the field line should be performed to obtain the wave structure along it, as well as the global wave growth rate. As the wave grows in

amplitude in the unstable region, it will propagate away along the field line to a higher-latitude location where its energy is absorbed by plasma via Landau or collisional damping processes. If the overall wave driving is stronger than the wave damping, the ICW will form an unstable eigenmode solution with the wave structure along the field line. From our experience on the nonlocal stability analysis, the wave amplitude is generally larger in the stronger local growth rate location. Because the observed wave frequency is rather coherent, in the saturation stage the ICW is expected to maintain its wave structure. The main nonlinear effect is due to a quasi-linear wave–particle interaction and velocity space spreading. Moreover, from the initial value simulations of ICWs, due to pickup ions in Saturn's magnetosphere (e.g., Cowee et al. 2009), the growth time of ICWs is more than 100 times longer than the ion cyclotron wave period. This means that the wave saturates, and its structure is maintained, so long as there is a constant pickup ion production rate. Thus, our conclusion on the ICW amplitude variation along the field line, based on the local growth rate, remains qualitatively valid.

Conclusion

Using the magnetic field data measured by the MAG instrument on board the Cassini satellite during 2005–2009, we have analyzed the nature of perturbed magnetic fields in the local water-group ion gyrofrequency range. We found that when the Cassini orbit is at low latitudes (near the equator) and inside 6 R_S, the observed waves are mostly transverse with left-hand circular polarization. We identify these waves as electromagnetic ion cyclotron waves (ICWs), destabilized by the pickup water-group ion velocity distribution. We have also investigated the spatial distribution of ICWs and found them to be located mostly inside 6 R_S of Saturn's magnetosphere. Inside 5.5 R_S the ion cyclotron wave distribution in latitude is wide (latitude: −20°–30°), but outside of 5.5 R_S it is narrower (latitude: −12°–12°). The ICW amplitude peaks at locations slightly off the equator (around ±1.5° to ±4° latitude). The theoretical analysis shows that the ICW growth rate reaches its maximum value at some critical n_0. The plasma density concentrates exponentially with distance along the field line toward the equator due to the plasma rotation. This means that the latitudinal variation of the ICW amplitude can be explained as occurring when the W^+ ion density decreases to the n_0 value at an off-equator magnetic latitude. However, there could be other reasons associated with the wave damping processes, such as collisional and Landau dampings. Because of the ICW latitudinal distribution, and the observation that the wave frequency at high latitude is smaller than the local ion gyrofrequency, we postulate that the ICWs are generated in the low-latitude region and propagate along the magnetic field line to the higher-latitude region.

The ICW amplitude is larger in the region between pre-midnight and dawn relative to other local time sectors. Also, the latitudinal distribution of the ICW amplitude and the latitude location of the peak amplitudes are local time dependent. This implies the local time dependence of the parallel ion temperature $T_{||}$, which drops from a few eVs in the midnight sector to below ~1 eV in the dusk sector. These values were estimated from the local stability theory by assuming a cold-ring distribution for the pickup ions and a Maxwellian distribution for the background thermal ions (note that $T_{||}$ values obtained in this paper are calculated from the axisymmetric rotating plasma equilibrium model and its values are only in qualitative agreement with the observed data). Based on this model, the July 26, 2009, MAG data imply a sudden increase in the ion temperature on that day. One possible reason for this is that Cassini was immersed in an ENA event. In addition, we conclude that the wave source can be located farther out than 6 R_S in the equatorial region, but that most of them are found in the midnight region. This indicates that the extra ion cyclotron wave driving sources (*e.g.*, the anisotropic velocity space distribution of ions) are due to physical processes other than the pickup ions near to the orbit of Enceladus. An extra ICW driving source of ion velocity space anisotropy may be due to ions which are brought into the inner magnetosphere on the nightside by plasma convection under disturbed conditions. This is similar to the plasma injection associated with substorms, magnetic reconnection, or other processes that take place in the Earth's magnetosphere. The ions come from the magnetotail then gradient-B drift eastward. Their velocity space anisotropy will thus be reduced as they drift around Saturn.

Authors' contributions

MC carried out the data analysis and numerical calculations, while CC derived the growth rate of ICWs. Both authors read and approved the final manuscript.

Author details

[1] Department of Physics, National Cheng Kung University, No. 1 University Road, Tainan 70101, Taiwan. [2] Institute of Space and Plasma Sciences, National Cheng Kung University, No. 1 University Road, Tainan 70101, Taiwan.

Acknowledgements

This work is supported by the National Science Council of Taiwan under Grant MOST 105-2111-M-006-001 and 105-2515-S-006-001.

Competing interests

The authors declare that they have no competing interests.

Publisher's Note

Received: 2 March 2017 Accepted: 25 August 2017
Published online: 07 September 2017

References

Barbosa DD (1993) Theory and observations of electromagnetic ion cyclotron waves in Saturn's inner magnetosphere. J Geophys Res 98:9345–9350. doi:10.1029/93JA00476

Blanco-Cano X (2004) Wave generation in moon–satellite interactions. Adv Space Res 33:2078–2091. doi:10.1016/j.asr.2003.03.033

Chou M, Cheng CZ (2010) Modeling of Saturn's magnetosphere during Voyager 1 and Voyager 2 encounters. J Geophys 115:A08202. doi:10.1029/2009JA015124

Cowee MM, Omidi N, Russell CT, Blanco-Cano X, Tokar RL (2009) Determining ion production rates near Saturn's extended neutral cloud from ion cyclotron wave amplitudes. J Geophys Res 114:A04219. doi:10.1029/2008JA013664

Dougherty MK, Magnetometer Team (2004) The Cassini magnetic field investigation: overview of arrival science. Space Sci Rev 114:331–383

Dougherty MK, Achilleos N, Andre N, Arridge CS, Balogh A, Bertucci C, Burton ME, Cowley SWH, Erdos G, Giampieri G, Glassmeier KH, Khurana KK, Leisner J, Neubauer F, Russell CT, Smith EJ, Southwood DJ, Tsurutani BT (2005) Cassini magnetometer observations during Saturn orbit insertion. Science 307:1266–1270. doi:10.1126/science.1106098

Hasegawa A (1969) Drift mirror instability of the magnetosphere. Phys Fluids 12:2642. doi:10.1063/1.1692407

Jia YD, Russell CT, Khurana KK, Leisner JS, Ma YJ, Dougherty MK (2010) Time-varying magnetospheric environment near Enceladus as seen by the Cassini magnetometer. Geophys Res Lett 37:L09203. doi:10.1029/2010GL042948

Johnson JR, Cheng CZ (1997) Global structure of mirror modes in the magnetosheath. J Geophys Res 102:7179. doi:10.1029/96JA03949

Leisner JS, Russell CT, Khurana KK, Dougherty MK, André N (2005) Warm flux tubes in the e-ring plasma torus: initial cassini magnetometer observations. Geophys Res Lett 32:L14S08. doi:10.1029/2005GL022652

Leisner JS, Russell CT, Dougherty MK, Blanco-Cano X, Strangeway RJ, Bertucci C (2006) Ion cyclotron waves in Saturn's E ring: initial Cassini observations. Geophys Res Lett 33:L11101. doi:10.1029/2005GL024875

Leisner JS, Russell CT, Dougherty MK, Persoon AM, Blanco-Cano X, McAndrews HJ, Thomsen MF, Strangeway RJ (2007) Energy flow in Saturn's ion cyclotron wave belt: 2007AGUFM.P43A1019L

Leisner JS, Russell CT, Wei HY, Dougherty MK (2011) Probing Saturn's ion cyclotron waves on high-inclination orbits: lessons for wave generation. J Geophys Res 116:3. doi:10.1029/2011JA016555

Russell CT, Blanco-Cano X (2007) Ion-cyclotron wave generation by planetary ion pickup. J Atmos Sol-Terr Phys 69:1723–1738. doi:10.1016/j.jastp.2007.02.014

Russell CT, Leisner JS, Arridge CS, Dougherty MK, Blanco-Cano X (2006) Nature of magnetic fluctuations in Saturn's middle magnetosphere. J Geophys Res 111:A12205. doi:10.1029/2006JA011921

Smith EJ, Tsurutani BT (1983) Saturn's magnetosphere: observations of ion cyclotron waves near the Dione L shell. J Geophys Res 88:7831–7836. doi:10.1029/JA088iA10p07831

Tokar RL, Wilson RJ, Johnson RE, Henderson MG, Thomsen MF, Cowee MM, Sittler EC Jr, Young DT, Crary FJ, McAndrews HJ, Smith HT (2008) Cassini detection of water-group pick-up ions in the Enceladus torus. Geophys Res Lett 35:L14202. doi:10.1029/2008GL034749

Wilson RJ, Tokar RL, Henderson MG, Hill TW, Thomsen MF, Pontius DH (2008) Cassini plasma spectrometer thermal ion measurements in Saturn's inner magnetosphere. J Geophys Res 113:A12218. doi:10.1029/2008JA013486